PROCEEDINGS, Twenty-Fifth Workshop on Geothermal Reservoir Engineering
Stanford University, Stanford, California, January 24-26, 2000
SGP-TR-165

FRACTURE ZONE CHARACTERIZATION IN GEOTHERMAL FIELD USING SATELLITE IMAGE, FLUID FLOW ANALYSIS, AND RADON PROSPECTING: A CASE STUDY OF THE ASO CALDERA, SOUTHWEST JAPAN

Katsuaki Koike[1),2)], Satoshi Tomita[1)], Tohru Yoshinaga[1)] and Michito Ohmi[1)]

[1] Faculty of Engineering, Kumamoto University, 2-39-1 Kurokami, Kumamoto 860-8555, Japan
e-mail: koike@gpo.kumamoto-u.ac.jp

[2] Visiting in Stanford Geothermal Program, Stanford University, Stanford, CA 94305-2220, USA
e-mail: koike@pangea.stanford.edu

ABSTRACT

Assemblage of main fracture and subordinate fractures form a fracture zone. Geometry, orientation, and permeability of fracture zone are significant factors for exploration and assessment of geothermal resources. Because these fracture attributes, which have an effect on the hydrothermal system represented by flow pattern and physical condition of hot fluids, are difficult to be clarified on a field scale, a combination of several methods is required for the fracture-zone characterization. This paper presents a case study of this characterization on the Aso caldera in southwestern Japan. The study consists of the three parts, lineament analysis, numerical simulation, and geophysical survey. Lineaments are derived from SPOT panchromatic imagery and used to calculate azimuths and dips of the major fractures associated with the origin of hot springs. A numerical simulation using finite element method is aimed at estimating the configuration and permeability of the fracture zone, formed by a gathering of the major fractures. By this calculation, the fracture zone was inferred to consist of two prisms that incline at angles of 70°-80° in the opposite direction of the mountain slope, and have permeability, 10^2 greater than that of the country, volcanic rocks. Moreover, the radon survey using scintillation counter method and soil gas near the fumaroles has been conducted to investigate the temporal changes of radon concentrations at the three sites, located on the two prisms. A difference in the temporal change patterns among the sites may result from the physical conditions of the hydrothermal fluids ascending through the prisms.

INTRODUCTION

Both the subsurface temperature and pressure distributions are indispensable factors for assessing the magnitude and potential of geothermal reservoirs. Because these distributions are closely related to the hydrothermal fluid flows, a regional flow analysis around the target site is required for reservoir characterization. Most of geothermal fields are located in mountainous terrains. Due to this geographical environment, the terrain is a main factor that controls the flow pattern and localizes the recharge and discharge areas. In addition to this, faults and continuous joints are believed to act as conduits for transporting the fluids (e.g., McCaig, 1989; Forster and Evans, 1991; Antonellini and Aydin, 1995; López and Smith, 1996) and also as geothermal reservoirs (e.g., Bodvarsson *et al*., 1982). We call these geological discontinuities "fractures" generically. Main fracture is not a single plane containing filling materials, but is mostly accompanied by damage zone (Caine *et al*., 1996) involving subordinate fractures and, in some cases, bounded by belts of anomalously low densities and seismic velocities zone extending a few kilometers (Stierman, 1984). These zones, formed by fracturing and chemical alteration, must have larger permeability than that of the surrounding rocks and emphasize the importance of themselves as major flow paths. It is significant, therefore, to estimate the location, geometry, and hydraulic property of the fracture zone for the regional flow analysis, with network modeling of fracture distribution (e.g., Long and Billaux, 1987; Koike and Kaneko, 1999).

This estimation is difficult in most cases because the fracture zones are generally concealed by thick superficial deposits. Boring core investigation is the most suitable for detecting the fracture characteristics such as density, orientation, aperture width, and displacement, and heterogeneous structures in the fracture zone may also be clarified by it. However, the information obtained by the boring survey is limited in both the amount and distribution. For elucidating the

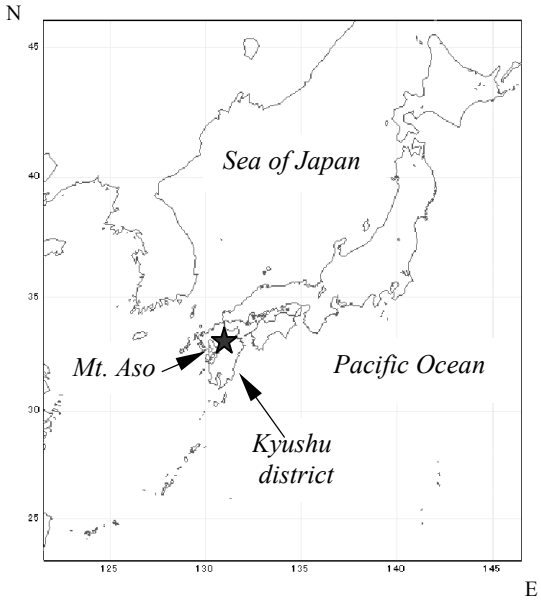

Fig. 1. Location of case study area, the Aso caldera, in southwestern Japan.

above characteristics of fracture zone, a combination of several analyses on the phenomena related to the fluid flows using remote sensing data, numerical simulation, and geophysical method is effective. This paper presents the combination and demonstrates its usefulness by a case study of an active volcano area in southwestern Japan.

STUDY AREA

The Kyushu district in southwestern Japan is known to be dominated by metalliferous deposits and active volcanoes, because the Daisen-Kirishima belt is located in the middle of the district. Mt. Aso, which has the biggest caldera in Japan, is situated nearly at the center of the Kyushu district (Fig. 1). This caldera was formed by one of the biggest eruption 90,000 years ago. The clarification of hydrothermal flow system in the caldera is important to the assessment of geothermal resources and the development with conserving the resources.

Mt. Aso mainly is overlain by andesitic and basaltic rocks of middle Pleistocene age. In the depths, the Permian and Triassic rocks of the Chichibu group, the Cretaceous granite, and the Mesozoic sedimentary rocks of the Mifune group are estimated to form the basement rocks. Because the altitude distribution of top of basement rocks is not known due to the lack of deep boring survey, we estimate it using the gravity anomaly data. The fracture-zone characterization is focused on the western slope of Mt. Aso. Three hot springs, Yunotani, Yoshioka, and Jigoku, are located on it as shown in Figs. 2 and 3.

LINEAMENT ANALYSIS

Lineaments are conspicuous features on both optical and microwave sensor images. Although lineament-interpretation ability is dependent upon illumination effects such as sun azimuth, imagery declination angle, and look direction, continuous faults and dominant joints appear as lineaments on the images. Therefore, lineament pattern provides basic information about tectonics and distribution of tectonically significant fractures. Lineaments correspond to straight or slightly curved edges defined by a series of adjacent pixels at the boundary of brightness changes. For automatic lineament extraction from the images, the segment tracing algorithm (STA) proposed by Koike *et al*. (1995) was employed. The purpose of the STA is to define a line composed of adjacent pixels as a vector element by examining local variance of gray level in the digital image and to connect retained line elements along their expected directions. Threshold values for the extraction and linkage of line elements are direction dependent in order to avoid the solar illumination bias. Some advantages of this method are its capability to (1) trace only continuous valleys and (2) extract more lineaments that parallel to the sun's azimuth and those located in shadow areas.

In addition to the lineament extraction, it is necessary, for lineament analysis aimed at clarification of geologic structures, to construct fracture planes and to estimate their strikes and dips. This can be carried out by the two steps: connection of several lineaments that are considered to belong to the same fracture system based on the criterion of distance and directional angle, and combination of lineament data with digital elevation model (DEM) (Koike *et al*., 1998). The appearance pattern of fractures on the terrain depends on their dip angles. This geometrical relationship can be described through vector analysis. According to the assumption of fracture shape being a plane with finite dimensions, we express a normal vector of a plane, $\boldsymbol{n}$. A slope is made by the DEM and its normal vector is represented by $\boldsymbol{t}_i$ (i = 1, 2, …, m), where m is the number of slopes through which the lineaments classified into the same group pass. Let the azimuthal vector of the lineament be $\boldsymbol{l}_i$. The $\boldsymbol{l}_i$ is equivalent to the intersection of the desired plane and the slope i. Therefore, the $\boldsymbol{l}_i$ should be equal to the vector product of two normal vectors:

$$\boldsymbol{l}_i = \boldsymbol{t}_i \times \boldsymbol{n} \quad (i = 1, 2, \ldots, m) \qquad (1)$$

The $\boldsymbol{n}$, the only unknown in this equation, can be obtained by applying the least-squares method and solving the normal equation (Koike *et al*. 1998).

SPOT panchromatic imagery, encompassing the hot spring areas, and the digital cartographic information of Japan with 250-m data spacing were used for the lineament analysis and DEM, respectively. Fig. 2

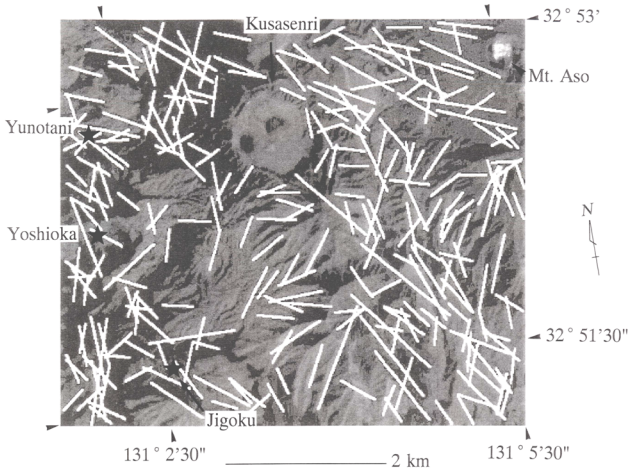

Fig. 2. Lineament map from STA overlaid with SPOT panchromatic image of Aso caldera. A star symbol indicates the location of hot spring.

shows the result of lineament extraction by the STA. The lengths of lineaments range from 0.3 to 1.5 km. From this map, the frequency of fractures striking north-northwest and northwest, which are the chief directions of ridges, is relatively inferred to be high. Several lineaments striking those directions pass the hot springs. A circular ancient crater called Kusasenri is located at the middle of the image (Fig. 2). There are no manifestations of hot springs on the eastern part of Kusasenri.

Fig. 3 illustrates the distribution of lineaments assumed to be related to the fractures existing around the hot springs. In order to show the subsurface fracture patterns, an east-west cross-section was constructed passing through the Jigoku hot spring area. The fractures located close to the hot springs are estimated to incline in the opposite direction of the mountain slope and have a steep dip angle, whereas the fracture located on the eastern side of Kusasenri possess westerly dip direction (Fig. 3(B)). The main source of hydrothermal fluids in the study area is rainwater. Because the terrain slopes roughly westward, it can be deduced that the two fractures dipping near the Jigoku hot spring area act as conduits for transporting hydrothermal fluids to the ground surface. The other fracture might provide a source of meteoric water.

NUMERICAL SIMULATION ON FLUID FLOW

In the study area, the hydrothermally altered zones are known to extend around the hot springs. This implies that the main fractures, detected by the lineament analysis, are connected and form a wide fracture zone. Fracture-zone characterization covers wide range of geological and geomechanical subjects. The origin of

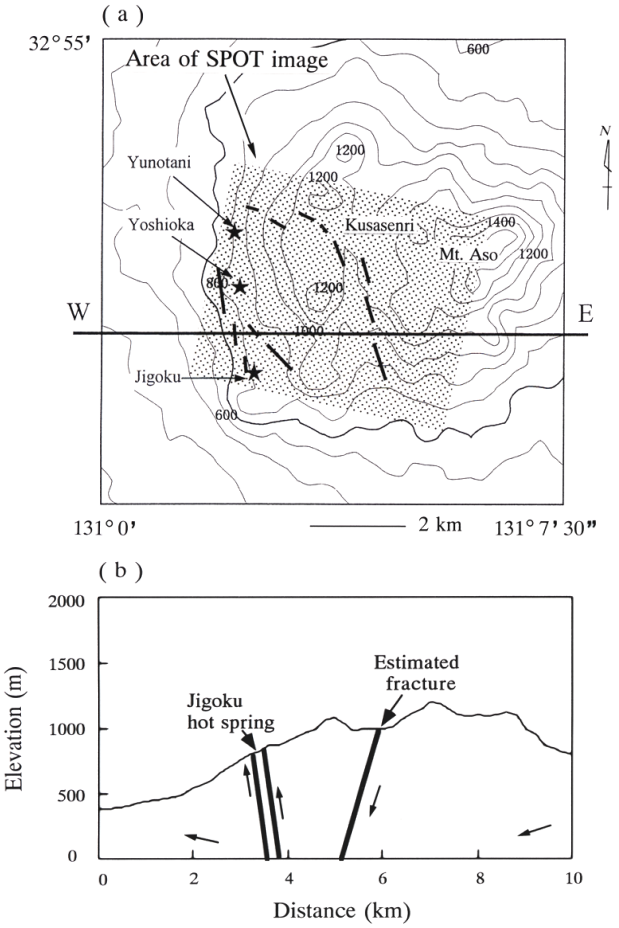

Fig. 3. (A) Locations of lineaments of three groups around hot springs. Thick line indicates location of cross section. (B) Cross section illustrating subsurface fracture patters. Arrows denote conjectured flow direction.

fracture is indeed an important problem to be investigated, but the estimations of permeability, dimensions, and shape are indispensable for evaluating the hydrogeologic significance of fracture zone. Though the lineament analysis is effective to elucidate dominant strikes and dips of major fracture planes, the hydrogeologic features of them cannot be detected from it. Accordingly, a numerical simulation is required for more detailed and quantitative analysis of hydrothermal system.

The fluid-flow pattern can be inferred from the pressure and temperature distributions. These physical quantities are calculated by a numerical simulation to obtain the solutions satisfying both the thermal energy balance and mass balance. To simplify the problem, we treated the fluid flow as single phase flow under the steady state following Hanaoka (1986). The governing equation for this case, simplified form of

the equation for the two phase and nonsteady flow by Faust and Mercer (1979), is:

$$\nabla\cdot\left[\frac{\mathbf{K}\rho}{\mu}\cdot\left(\nabla P-\rho g\nabla Z\right)\right]+q_m=0 \tag{2}$$

$$\nabla\cdot\left[\frac{\mathbf{K}\rho}{\mu}h\cdot\left(\nabla P-\rho g\nabla Z\right)\right]+\nabla\cdot\left[K_m\left(\frac{\partial T}{\partial h}\right)_P\nabla h\right]+q_h=0$$

where P, g, ρ, μ, $\mathbf{K}$, Z, q_m, q_h, h, K_m, and T denotes pressure, gravitational acceleration, density, viscosity, permeability, depth, mass flux, heat flux, enthalpy, thermal conductivity, and temperature, respectively. The flow is assumed to follow Darcy's law.

$$\mathbf{v}=-\frac{\mathbf{K}}{\mu}\left(\nabla P-\rho g\nabla Z\right) \tag{3}$$

where $\mathbf{v}$ is flow velocity. A three-dimensional finite element method was applied to the calculation.

The calculation covers the area of 10 km by 10 km and the vertical range from the ground surface to the altitude –2 km. This region was divided by elements of tetrahedron shape as shown in Fig. 4. The elevations of the ground surface were given using the DEM and the elevation at each nod on the surface was supposed to be equal to the groudwater table. This simulation model is simply composed of two layers: the volcanic rocks and basement rocks are assigned to the upper and lower layers as the major lithology. Total numbers of nods and elements are 18,490 and 95,256. The boundary conditions are the follows. The surface temperature was kept at 10°C, while the temperatures at the bottom plane were given by thermal gradient of 0.05°C/m. Heat transfer was prohibited at the vertical boundary planes. The pressures at the surface plane were supposed to be

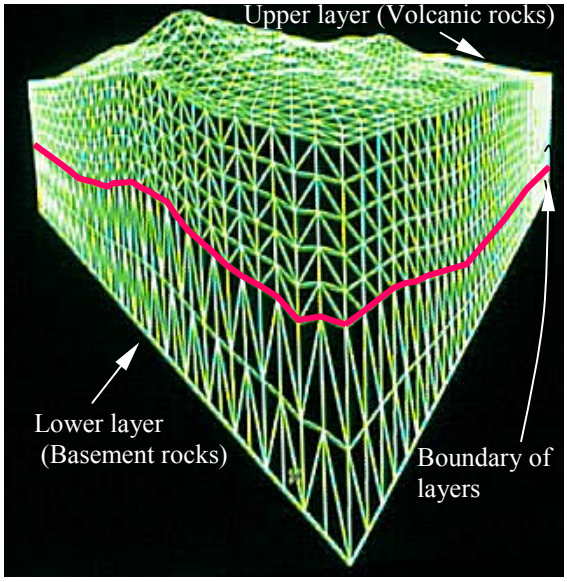

Fig. 4. Geometry of elements used in 3-D finite element method for fluid –flow analysis.

equal to the atmospheric pressure and the impermeable condition was given to the other boundary planes. It is important to appropriately presume the permeability and thermal conductivity for the two layers. These were defined as 1.0×10^{-18} m^2 and 5.0 W/m°C for the basement rocks, and 1.0×10^{-16} m^2 and 3.0 W/m°C for the volcanic rocks by referring to the measurement data of Yano (1985).

The estimation of permeability of fracture zone is a difficult problem because it varies widely between 10^{-12} m^2 and 10^{-22} m^2 (Caine *et al*., 1996) according to the various factors such as magnitude of confining pressure, width, kind and condition of filling materials, regional tectonic stress, and history of tectonic movement. However, many researches have proven the general role of fracture zone as flow path, with larger permeability than that of surrounding rocks. Thus, we firstly attempted to execute the calculations by placing a planer fracture zone from the Yunotani to the Jigoku and defining a larger permeability than that of the volcanic and basement rocks. However, this model could not produce any increase of temperatures in the shallow depths at the hot springs. The reason may be that the defined fracture zone is too continuous and enhances selectively descending flows.

Next, we assumed that the fracture zone is composed of two subareas: zone A including the Yunotani and Yoshioka, and zone B including the Jigoku. Both of these zones were estimated to dip eastward based on the result of lineament analysis. The definition of two zones merely was not sufficient to produce a proper temperature distribution. Moreover, we presumed that a sub volcanic conduit, branched from the main one, is existed in the fracture zone, and defined the temperatures at the sub volcanic conduit on the bottom plane of the model by thermal gradient of 0.1°C/m. This part specified on the bottom plane is called heat source hereafter. The dimensions, permeability, and dip angle of the fracture zone influence the temperature distribution and fluid-flow pattern, with the dimensions and location of the heat source. These unknown parameters were determined by comparing the calculated temperatures with the temperature profile to the 400-m depth at the Yunotani and making remarkable ascent flows through the fracture zones. As a result, suitable pattern was obtained by: 1500 m×1500 m cross-section area and permeability of 10^{-14} m^2 for both the fracture zones, 1000 m×500 m area for the heat source, and the western side in the fracture zone for the location of heat source. The thermal conductivity of the fracture zone was defined as 3.0 W/m°C. The dip angles of zone A and B are 80° and 70°. Fig. 5 illustrates the fracture zone model in shape of prism and the location of heat source.

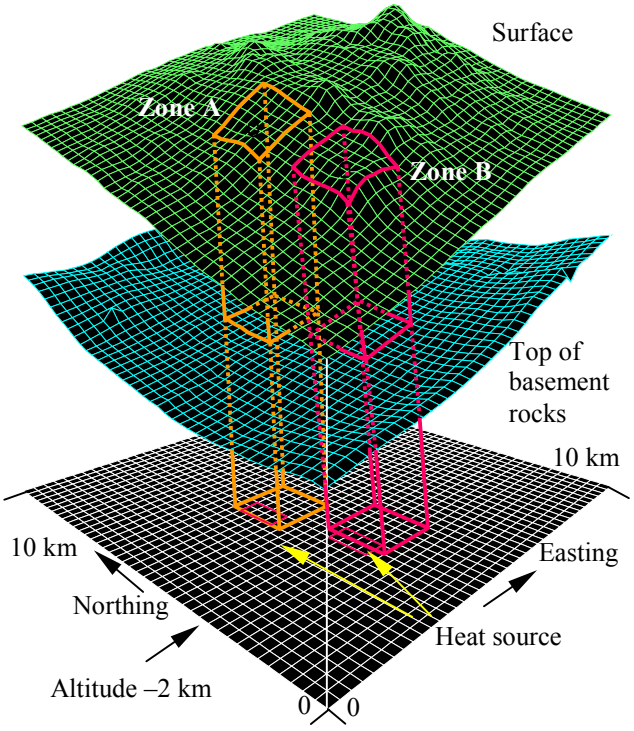

Fig. 5. Fracture zone model having a role as conduit for fluid flows and location of heat source.

Fig. 6 shows a vertical cross-section of the calculated temperature distribution and flow pattern by isothermal lines and flow vectors. The cross-section is selected along an east-west line passing through the Yunotani area. In the eastern part of the Yunotani area, the descending flows are dominant and the temperatures are generally low, as inferred from the result of lineament analysis (Fig. 3(B)). Opposite from it, the ascending flows are conspicuous near the hot spring and the temperatures at shallow depths become high with the flows.

RADON SURVEY USING SOIL GAS FOR TRACING FLUID CONDITION

The fracture zone is characterized from the viewpoint of the effect of its existence on the physical condition of fluid flows. Because it is difficult to directly measure the condition, radon, which is noble gas and easily detected by *in situ* test, was selected as an indicator of fluid condition. The effectiveness of radon as an *in situ* tracer of geothermal reservoirs was demonstrated by Semprini and Kruger (1984).

We adopted α-scintillation counter method for the radon survey and used RDA-200 radon detector (Syntrex Inc.). A hole of 1-m depth and 3-cm diameter was dug and protected by a vinyl chloride pipe. The detector counts the number of α particles in one minute successively. The α particle is emanated with the decays of ^{222}Rn, ^{220}Rn, ^{218}Po, and ^{216}Po. ^{218}Po and ^{216}Po are daughter nuclides of ^{222}Rn and ^{220}Rn, respectively. From the 20-minute data, we estimate the radon concentration using the calculation method of number of radon atoms (CMNR: Koike *et al.*, 1996). The CMNR considers the soil-gas condition with respect to the radioactive equilibrium.

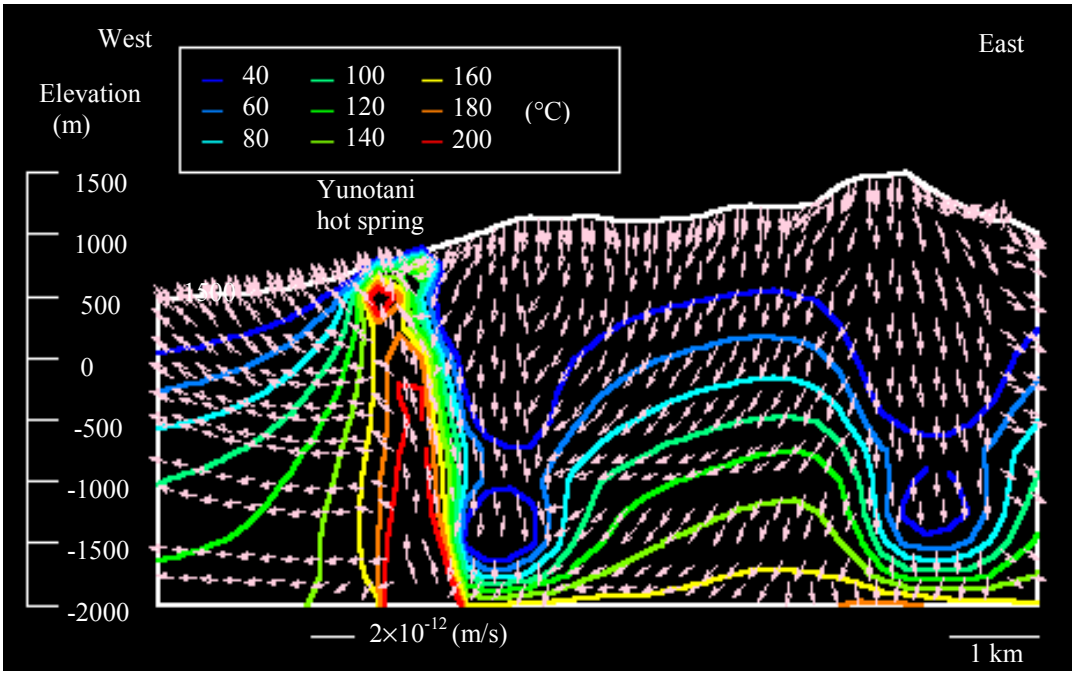

Fig. 6. Cross-section showing calculated temperature distribution and flow vectors along an E-W line passing through the Yunotani hot spring area.

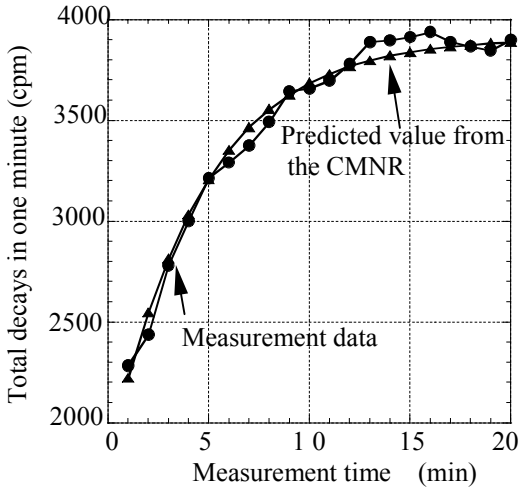

Fig. 7. Typical measurement data showing radon decays in each one minute under the radioactive nonequilibrium condition.

For the nonequilibrium condition, the total decays, V_k, from $t=T_a+\tau_{k-1}$ to $t=T_a+\tau_k$ is expressed by

$$V_k = \lambda_{222}\left[2\Delta t + \frac{\lambda_{222}\Delta t - \exp(-\lambda_{218}\tau_{k-1}) + \exp(-\lambda_{218}\tau_k)}{\lambda_{218}-\lambda_{222}}\right]N_{222} + \left[\exp(-\lambda_{218}\tau_{k-1}) - \exp(-\lambda_{218}\tau_k)\right]N_{218} + 2\left[\exp(-\lambda_{220}\tau_{k-1}) - \exp(-\lambda_{220}\tau_k)\right]N_{220} \quad (4)$$

where T_a is the age of radon gas; $\tau_k = k\Delta t$ (k=1, … , n: n is the number of measurements andΔt is the time interval of a measurement) is the time difference between the T_a and each minute of measurement; N_{222}, N_{218}, and N_{220} are the number of atoms of ^{222}Rn, ^{218}Po, and ^{220}Rn at the start of measurement; and λ_{222}, λ_{218}, and λ_{220} are the decay constants of these nuclides. The T_a (≤1980 sec) can be calculated using the N_{222} and N_{218}. For the gas that has reached the equilibrium condition (T_a>1980 sec), the V_k is expressed by

$$V_k = (2+r)\left[\exp(-\lambda_{222}\tau_{k-1}) - \exp(-\lambda_{222}\tau_k)\right]N_{222} + 2\left[\exp(-\lambda_{220}\tau_{k-1}) - \exp(-\lambda_{220}\tau_k)\right]N_{220} \quad (5)$$

where $r=\lambda_{222}/\lambda_{218}$ and $N_{218}=rN_{220}$. The N_{222}, N_{218}, and N_{220} can be obtained through the least-squares analysis of V_k for both the conditions. The N_{222} is the important factor to consider the physical conditions of the soil gas and hydrothermal fluids, because the half-life of ^{222}Rn (3.83 days) is 6,000 times as long as that of ^{220}Rn. For this reason, the N_{222} is called radon concentration hereafter.

The radon survey, including the measurements of temperature, atmospheric pressure, and 1-m depth temperature, started in May 1994 and has continued at the rate of once a week. The measurement holes were established near the fumaroles in the three hot springs. Fig. 7 shows an example of temporal changes of radon

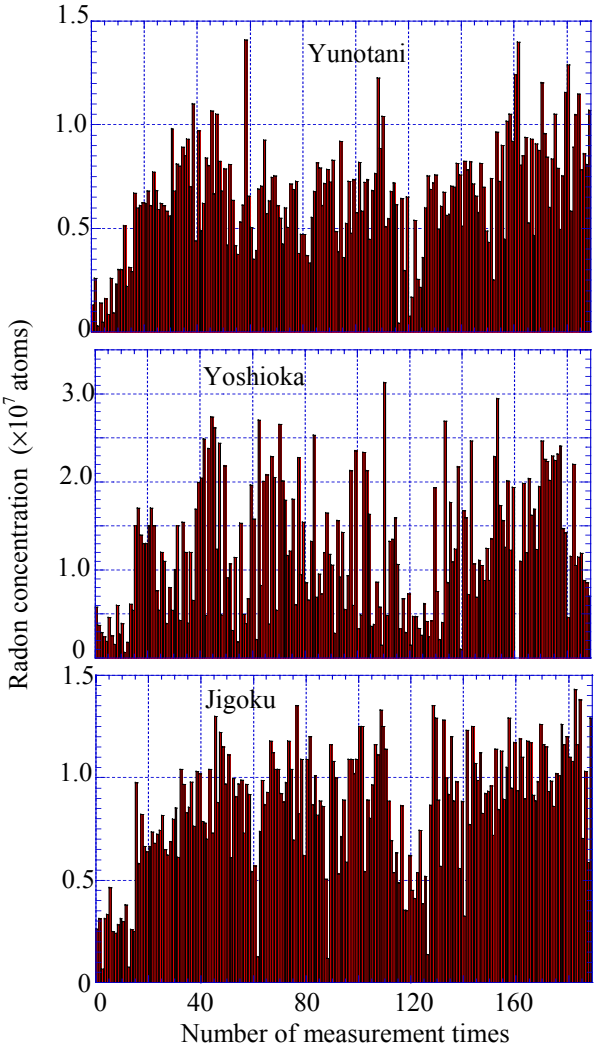

Fig. 8. Temporal changes of radon concentrations over four years at the three hot springs.

decays in minute under the radioactive nonequilibrium condition, which represents increase of the number of decays with the time. The numbers of radon decays predicted from the CMNR are compared to the measurement data as shown in Fig. 7. It can be confirmed that they agree with each other. The temporal changes of the radon concentration over four years at the three areas are shown in Fig. 8. The radon concentrations were found to have low correlation with the meteoric conditions such as precipitation, temperature, and 1-m depth temperature except the data of Yoshioka. With respect to the general trend of the radon concentrations, the three areas have similar periodicity, phase, and change pattern. This similarity may result from the tectonic environment that these areas are located on the same fracture system. However, the amplitudes of concentration changes are different among the three. The Yoshioka has the largest variations influenced by the weather conditions, whereas the radon concentrations at the

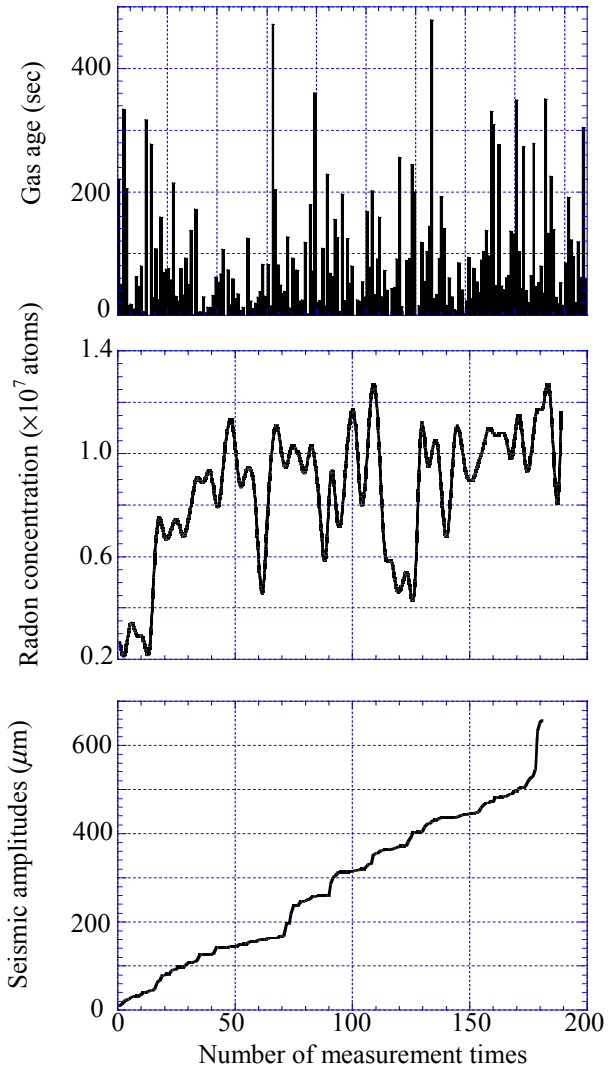

Fig. 9. Temporal changes of gas age and radon concentration at the Jigoku and cumulative distribution of amplitudes of volcanic seismicity in the Aso caldera.

Jigoku correspond well to the volcanic seismicity among the three.

Fig. 9 depicts the temporal changes of the age of radon gas and the radon concentration approximated by a spline curve to identify general trend at the Jigoku, and the cumulative distribution of amplitudes of volcanic seismicity observed in the Aso caldera. The radon concentration and the gas age seem to become large and young, respectively, when the seismicity becomes active. Because radium, parent nuclide of radon, is considered to be uniformly distributed in the fluids, the radon concentration is influenced by the temperature and pressure changes of the hydrothermal fluids associated with the seismic activity.

DISCUSSION ON PHYSICAL CONDITION OF FLUIDS THROUGH THE FRACTURE ZONE

In active volcanoes, some of earthquakes have genetic relation to uplift of magma body. The same mechanism is applied to Mt. Aso: the activation of volcanic seismicity is presumed to be caused by the uplift of magma body, which may specifically increase the thermal gradient at the heat source. Fig. 10 shows the changes of pressure and temperature at the nodes located in the fracture zone and on the surface of basement rocks, with the thermal gradient between 0.09 and 0.1 °C/m. The surface altitudes in the two fracture zones are roughly the same. Because the flow velocity is small, the influence of the physical changes of hydrothermal fluids at deep depths takes long time to be appeared near the ground surface. Therefore, the change of radon concentration may be caused by the carrier gases, which are separated from the fluids at deep depths and ascend at high speed. This is reason for selecting the above-mentioned nods. From Fig. 10, similar trends of the pressure changes are found between the zones A and B: the pressure decreases

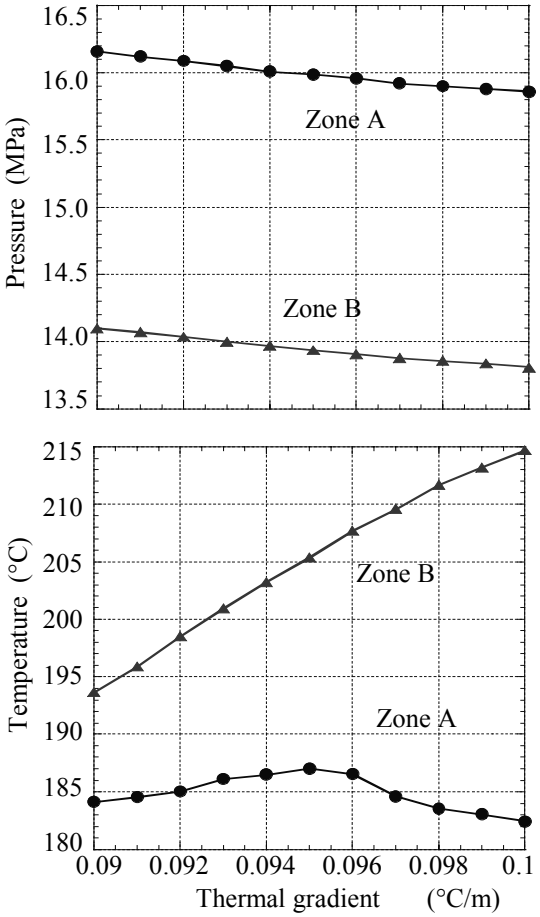

Fig. 10. Changes of pressure and temperature at nodes located on the surface of basement rocks in the zones A and B, with increase of thermal gradient at heat source.

with the increase of thermal gradient. On the contrary, there is a difference in the temperature changes: the temperature increases monotonously with the increase of thermal gradient in the zone B, while it takes a maximum at 0.095 °C/m and decreases at the larger values than it in the zone A. In addition, the zone B has lower pressure and higher temperature as compared with the zone A, which effectively operates to lower the dissolved radon concentration and degas the fluids. These fluid characteristics can be a factor for the radon concentrations at the Jigoku located in the zone B, which are higher than the Yunotani and fluctuate corresponding to the volcanic seismicity. The existence of fracture zones A and B, with the terrain of Mt. Aso, may produce some parts of the estimated fluid characteristics.

CONCLUSIONS

A combination of the lineament analysis, the numerical simulation on fluid flow, and the radon survey using soil gas near the fumaroles was examined for the fracture-zone characterization. The lineament analysis using the satellite image and DEM was proved to be capable of elucidating the dominant strikes and dips of major fracture planes. The numerical simulation is necessary for evaluating hydrogeologic features of fracture zone, represented by geometry, orientation, and permeability. For the case study area located in the Aso caldera, the fracture zone that localizes the three hot springs was inferred to consist of two prisms inclining at angles of 70°-80° in the opposite direction of the mountain slope, and have permeability, 10^2 greater than that of the surrounding, volcanic rocks. The radon survey was carried out to demonstrate that the physical conditions of the fluid flows might be related to the existence of fracture zone. Though the general trends of temporal changes of radon concentrations were similar, the amplitudes of concentration changes were found to differ among the three hot springs. This phenomena is considered to result from the difference in response of hydrothermal fluids through the fracture zone to the external disturbance such as volcanic seismicity. Consequently, the proposed combination is effective to detect the characteristics of both the fracture zone and the physical conditions of fluid flows ascending through the zone.

REFERENCES

Antonellini, M. and Aydin, A. (1995) "Effect of Faulting on Fluid Flow in Porous Sandstones: Geometry and Spatial Distribution," *AAPG Bulletin*, **79**, 642-671.

Bodvarsson, G. S., Benson, S. M. and Witherspoon, P. A. (1982) "Theory of the Development of Geothermal Systems Charged by Vertical Faults," *J. Geophys. Res.*, **87**, 9317-9328.

Caine, J. S., Evans, J. P. and Forster, C. B. (1996) "Fault Zone Architecture and Permeability Structure," *Geology*, **24**, 1025-1028.

Faust, C. R. and Mercer, J. W. (1979) "Geothermal Reservoir Simulation 1. Mathematical Models for Liquid- and Vapor-Dominated Hydrothermal Systems," *Water Resour. Res.*, **15**, 23-30.

Forster, C. B. and Evans, J. P. (1991) "Hydrogeology of Trust Faults and Crystalline Thrust Sheets: Results of Combined Field and Modeling Studies," *Geophys. Res. Lett.*, 18, 979-982.

Hanaoka, M. (1986) "Structural Control Hydrothermal System by Gravity Basement," *J. Geothermal Research Society of Japan*, **8**, 379-412 (in Japanese with English abs.).

Koike, K., Nagano, S. and Ohmi, M. (1995) "Lineament Analysis of Satellite Images Using a Segment Tracing Algorithm (STA)," *Computers & Geosciences*, **21**, 1091-1104.

Koike, K., Kawaba, K., Yoshinaga, T. and Ohmi, M. (1996) "Characterization of Latent Fault Based on Soil Radon Concentration," *Jap. J. Geophys. Exploration*, **49**, 347-359 (in Japanese with English abs.).

Koike, K., Nagano, S. and Kawaba, K. (1998) "Construction and Analysis of Interpreted Fracture Planes Through Combination of Satellite-Image Derived Lineaments and Digital Elevation Model Data," *Computers & Geosciences*, **24**, 573-583.

Koike, K. and Kaneko, K. (1999) "Characterization and Modeling of Fracture Distribution in Rock Mass Using Fractal Theory," *Geothermal Science and Technology*, **6**, 43-62.

Long, J. C. S. and Billaux, D. M. (1987) "From Field Data to Fracture Network Modeling: An Example Incorporating Spatial Structure," *Water Resour. Res.*, **23**, 1201-1216.

López, D. L. and Smith, L. (1996) "Fluid Flow in Fault Zones: Influence of Hydraulic Anisotropy and Heterogeneity on the Fluid Flow and Heat Transfer Regime", *Water Resour. Res.*, **32**, 3227-3235.

McCaig, A. M. (1989) "Fluid Flow Through Fault Zones," *Nature*, **340**, 600.

Semprini, L. and Kruger, P. (1984) "Relationship of Radon Concentration to Spatial and Temporal Variations of Reservoir Thermodynamic Conditions in the Cerro Prieto Geothermal Field," *Geothermics*, **13**, 103-115.

Stierman, D. J. (1984) "Geophysical and Geological Evidence for Fracturing, Water Circulation and Chemical Alteration in Granitic Rocks Adjacent to Major Strike-Slip Fault," *J. Geophys. Res.*, 89, 5849-5856.

Yano, Y. (1985), "Analysis of Hydrothermal System Using Well Data in the Hohi Geothermal Area," *Report Geol. Surv. Japan*, **264**, 385-404 (in Japanese with English abs.).